

# 1 **High-frequency quantitative ultrasound to assess the acoustic** 2 **properties of engineered tissues in vitro**

3 **Authors:** Joseph A. Sebastian<sup>1,2</sup>, Eric M. Strohm<sup>3,4,5</sup>, Emmanuel Chérin<sup>6</sup>, Bahram Mirani<sup>1,2,7</sup>,  
4 Christine Démore<sup>6,8</sup>, Michael C. Kolios<sup>3,4,5</sup>, Craig A. Simmons<sup>1,2,7</sup>

## 5 **Affiliations:**

- 6 1. Institute of Biomedical Engineering, University of Toronto, Toronto, Canada
- 7 2. Translational Biology and Engineering Program, Ted Rogers Center for Heart Research,  
8 Toronto, Canada
- 9 3. Department of Physics, Toronto Metropolitan University, Toronto, Canada
- 10 4. Institute of Biomedical Engineering, Science and Technology (iBEST), a partnership  
11 between Toronto Metropolitan University and St. Michael's Hospital, Toronto, Canada
- 12 5. Keenan Research Centre for Biomedical Science, Li Ka Shing Knowledge Institute, St.  
13 Michael's Hospital, Toronto, Canada
- 14 6. Sunnybrook Research Institute, Toronto, Canada
- 15 7. Department of Mechanical and Industrial Engineering, University of Toronto, Toronto,  
16 Canada
- 17 8. Department of Medical Biophysics, University of Toronto, Toronto, Canada

18 \*Address correspondence to: [c.simmons@utoronto.ca](mailto:c.simmons@utoronto.ca) or [j.sebastian@mail.utoronto.ca](mailto:j.sebastian@mail.utoronto.ca)

19 **KEYWORDS:** Hydrogels, engineered tissues, high-frequency ultrasound, acoustic attenuation,  
20 cell-seeded biomaterials

21

## 22 **Abstract**

23 Acoustic properties of biomaterials and engineered tissues reflect their structure and cellularity.  
24 High-frequency ultrasound (US) can non-invasively characterize and monitor these properties with  
25 sub-millimetre resolution. We present an approach to estimate the acoustic properties of cell-laden  
26 hydrogels that accounts for frequency-dependent effects of attenuation in coupling media,  
27 hydrogel thickness, and interfacial transmission/reflection coefficients of US waves, all of which  
28 can bias attenuation estimates. Cell-seeded fibrin hydrogel disks were raster-scanned using a 40  
29 MHz US transducer. Thickness, speed of sound, acoustic impedance, and acoustic attenuation  
30 coefficients were determined from the difference in the time-of-flight and ratios of the magnitudes  
31 of US signals, interfacial transmission/reflection coefficients, and acoustic properties of the  
32 coupling media. With this approach, hydrogel thickness was accurately measured by US, with  
33 excellent agreement to confocal microscopy ( $r^2 = 0.97$ ). Accurate thickness measurement enabled  
34 acoustic property measurements that were independent of hydrogel thickness, despite up to 60%  
35 reduction in thickness due to cell-mediated contraction. Notably, acoustic attenuation coefficients  
36 increased with increasing cell concentration ( $p < 0.001$ ), reflecting hydrogel cellularity independent  
37 of contracted hydrogel thickness. This approach enables accurate measurement of the intrinsic  
38 acoustic properties of biomaterials and engineered tissues to provide new insights into their  
39 structure and cellularity.

40

## 41 **1 Introduction**

42           Ultrasound (US) is an emerging measurement technique in biomaterials and tissue  
43 engineering (TE) applications due to its non-invasive, non-destructive, and real-time monitoring  
44 capabilities [1-5]. Beyond its well-known imaging capabilities, US can also be used to measure  
45 acoustic properties related to structural, functional, and intrinsic material properties of interest for  
46 biomaterials and engineered tissue applications. For example, US measurements of the speed of  
47 sound, acoustic impedance, and acoustic attenuation in a biomaterial correlate with the material's  
48 microstructure [6], elastic properties [7], and cellularity [8, 9], respectively.

49           High frequency US (>10 MHz) is particularly attractive for in vitro TE applications, as it  
50 offers sub-millimetre spatial resolution to enable tissue- and cell-scale measurements (at tens and  
51 hundreds of MHz, respectively). However, a particular challenge with the application of US in  
52 these applications at high frequencies is that the bandwidth of the US transducers is large, the  
53 attenuation high, and the relationship between attenuation and frequency can become non-linear.  
54 Thus, an accurate estimation of the acoustic attenuation of biological media at high frequencies is  
55 critical to determining other acoustic properties (e.g., backscatter coefficient) and inferring the  
56 material properties of engineered tissues and cells.

57           In previous studies, attenuation in biological samples was estimated using a substitution  
58 method, whereby the US signals propagating between two transducers [7, 8, 10, 11], or reflected  
59 from a reference substrate (e.g., quartz) [12-14], were acquired in the presence and absence of the  
60 sample in the US path, and their amplitudes compared in either the time- and/or frequency-domain.  
61 However, as implemented in these studies, the method fails to fully compensate for the attenuation  
62 in the coupling medium, for the transmission of US waves at the coupling medium-biomaterial  
63 interface and, when required, for the reflection at the biomaterial-substrate interface. If not

64 compensated for, transmission and/or reflection coefficients at interfaces introduce a bias in the  
65 estimate of the sample attenuation coefficient. This bias increases with the difference in acoustic  
66 impedance between the sample and coupling medium and is inversely proportional to the sample  
67 thickness. This bias becomes significant for attenuation measurements in thin samples and/or for  
68 significant differences in impedance between media. Furthermore, the sample thickness is often  
69 assumed based on sample preparation [8,9,11], which fails to account for dynamic reorganization  
70 of biomaterials by embedded cells that can alter thickness [15] and consequently affect the  
71 attenuation coefficient estimate. As an alternative to substitution methods, Ruland et al. [16, 17]  
72 recently introduced a reference phantom method (RPM) for quantitative US of cell-laden  
73 hydrogels and bioscaffolds. In the RPM, a sample's acoustic properties are determined by  
74 comparison to a reference phantom of known attenuation and sound speed. However, this approach  
75 is limited to samples with similar acoustic properties to the RPM and also does not account for  
76 cell-mediated effects on the biomaterial shape and size and their effect on acoustic properties, and  
77 thus would be challenging to implement to track dynamic changes. Thus, compensation for  
78 transmission/reflection at interfaces and measurement of the biomaterial sample thickness is  
79 critical for accurately determining its acoustic attenuation coefficient and microstructural  
80 assessment.

81 Here, we present an US method of estimation of the thickness and acoustic properties of  
82 engineered tissues. We benchmarked this technique against published acoustic property values of  
83 polymethylpentene (TPX). This method accounts for the frequency- and thickness-dependent  
84 effects of attenuation in the coupling medium and reflection/transmission of US waves at  
85 interfaces. We demonstrate thickness-independent measurement of the speed of sound, acoustic  
86 impedance, and acoustic attenuation coefficient of fibrin hydrogels as a model biomaterial, at four

87 different cell densities (cell-free control,  $1 \times 10^5$ ,  $1 \times 10^6$ , or  $1 \times 10^7$  cell/ml) and three different initial  
88 thicknesses (1.25 mm, 1.00 mm, 0.75 mm). From the estimated acoustic properties, we derive the  
89 density and elastic modulus of the cell-laden hydrogels.

## 90 **2 Methods**

### 91 **2.1 Acoustic characterization**

92 Acoustic properties of samples were estimated at high frequency using a substitution method  
93 adapted from Briggs et al. [18] and depicted in Fig. 1A. US echoes reflected from the substrate  
94 surface (polystyrene in our case) with and without the sample inserted in the propagation path and  
95 reflected from the surface of the sample ( $s_2(t)$ ,  $s_1(t)$  and  $s_3(t)$ , respectively) are collected. Their  
96 Fourier transforms  $S_i(f)$  ( $i = 1, \dots, 3$ ) are calculated to evaluate, in the frequency domain  
97 (Supplementary Figure 1), the coefficients of reflection ( $R_{w-s}$ ) and transmission ( $T_{w-s}$ ) at the  
98 water-sample interface, the coefficient of reflection ( $R_{w-p}$ ) at the water-substrate interface, and  
99 the coefficient of reflection ( $R_{s-p}$ ) at the sample-substrate interface. These coefficients are  
100 compensated for in equation (1), to get an unbiased estimation of the frequency-dependent  
101 attenuation in the sample  $\alpha_s$  (Supplementary Figure 1):

102

$$103 \quad \alpha_s(f) = \alpha_w(f) + \frac{1}{2d} \cdot 20 \log_{10} \left[ \frac{S_1(f)}{R_{w-p}} \cdot \frac{R_{s-p}(f)}{S_2(f)} \cdot T_{w-s}^2(f) \right] \quad (1)$$

104 where:

$$105 \quad T_{w-s}^2(f) = 1 - R_{w-s}^2(f) \quad (2)$$

106 with:

$$107 \quad R_{w-s}(f) = R_{w-p} \frac{S_3(f)}{S_1(f)} \quad (3)$$

108 
$$R_{w-p} = \frac{Z_p - Z_w}{Z_p + Z_w} \quad (4)$$

109 In equation (4),  $Z_w$  and  $Z_p$  are the acoustic impedances of water and the polystyrene  
110 substrate, respectively, and known. The reflection coefficient at the sample-substrate interface  
111  $R_{s-p}$  in equation (1) is calculated from  $Z_p$  and the acoustic impedance of the sample  $Z_s$ :

112 
$$R_{s-p}(f) = \frac{Z_p - Z_s(f)}{Z_p + Z_s(f)} \quad (5)$$

113 with:

114 
$$Z_s(f) = Z_w \frac{1 + R_{w-s}(f)}{1 - R_{w-s}(f)} \quad (6)$$

115 The thickness of the sample  $d$  is estimated from the difference in time of flight  $\Delta t$  between  
116 the echo from the uncovered substrate  $s_1(t)$  and the echo from the top of the phantom (Fig. 1A,  
117 green arrow) while focusing on the substrate, and the speed of sound in water  $c_w$ :

118 
$$d = c_w \frac{\Delta t}{2} \quad (7)$$

119 Time of flight was estimated as the times at which the peaks of the envelope of these echoes  
120 ( $s_1(t)$  and  $s_3(t)$ ) were detected relative to US pulse transmission. Finally, since the logarithmic  
121 term in equation (1) corresponds, once normalized to the sample thickness, to the difference in  
122 attenuation between sample and water, water attenuation  $\alpha_w$  is added to calculate the attenuation  
123 in the sample  $\alpha_s$ .

124 The speed of sound in the sample can be calculated from the thickness of the sample  
125 estimated in (7), and the difference in time of flight  $\Delta t'$  between the echo from the surface of the  
126 sample (Fig. 1A, green arrow) and the echo from the underlying substrate  $s_2(t)$ :

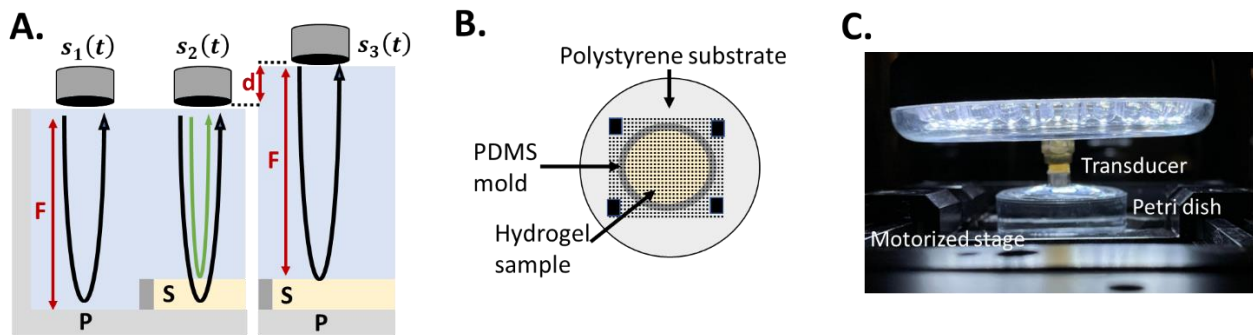
127 
$$c_s = \frac{2d}{\Delta t'} \quad (8)$$

128 Finally, the sample density  $\rho_s$  and elastic modulus  $\varepsilon_s$  can be estimated from the sample  
129 acoustic impedance and speed of sound, and speed of sound and density, respectively:

130 
$$\rho_s = \frac{Z_s}{c_s} \quad (9)$$

131 
$$\varepsilon_s = \rho_s c_s^2 \quad (10)$$

132



133

134 **Figure 1:** (A) Schematic representing the experimental system used to estimate the sample  
135 acoustic properties where S is the sample, P is the polystyrene substrate, F is the focal distance of  
136 the 40 MHz transducer, and  $d$  is sample thickness.  $s_1(t)$  is the signal collected from the substrate  
137 surface (polystyrene in our case),  $s_2(t)$  is the signal collected with the sample inserted in the  
138 propagation path, and  $s_3(t)$  is the signal reflected from the surface of the sample.  $s_1(t)$  and  $s_2(t)$   
139 are measured together (see description in B.) and  $s_3(t)$  is measured separately. The thickness of  
140 the sample  $d$  is estimated from the difference in time of flight between the echo from the uncovered  
141 substrate  $s_1(t)$  and the echo from the top of the phantom (green arrow) while focusing on the  
142 substrate. (B) Top view of a hydrogel sample cast in an 8 mm diameter polydimethylsiloxane mold  
143 positioned in the polystyrene Petri dish. The overlaid dotted lines represent the 15 mm x 15 mm  
144 raster scan with 100 μm step size in the x- and y-directions for the ultrasound measurements. The  
145 black squares represent the region where  $s_1(t)$  was acquired. (C) Picture of the imaging system  
146 with the front face of the ultrasound transducer immersed into the polystyrene Petri dish filled with  
147 water.

148

## 149 2.2 High-frequency ultrasound system and signal acquisition

150 A custom-built US system was developed to acquire ultrasound signals from the sample  
151 and substrate. This system comprises a single-element spherically focused 40-MHz transducer  
152 (focal distance  $F=8.56$  mm, f-number 3) providing a 36 μm axial resolution, 110 μm lateral

153 resolution (in the focal zone), and 4 mm depth-of-field (all measured at -6 dB) using a 40- $\mu$ m  
154 aperture needle hydrophone (NH0040, Precision Acoustics Ltd, Dorchester, U.K.). The transducer  
155 was affixed to a microscope (IX71, Olympus America Inc., Melville, NY) equipped with a 3D-  
156 motion stage (Prior Scientific, USA; 2 motorized lateral axes X and Y, 1 manual vertical axis Z)  
157 on which the sample was positioned in a polystyrene Petri dish (Greiner Bio-One, North Carolina,  
158 USA), covered with water. The sample was moved relative to the transducer in a raster scan  
159 manner with a 100  $\mu$ m step size in both lateral directions and such that a 15 mm x 15 mm region  
160 of interest (ROI). The ROI incorporated the sample, underlying substrate, and some uncovered  
161 substrate (Fig. 1B). US signals  $s_1(t)$ ,  $s_2(t)$  and  $s_3(t)$  (Fig. 1A) were acquired at each lateral  
162 position  $(x, y)$ , in two separate raster scans. For these acquisitions, monocycle pulses generated  
163 by a pulse generator (AVB2-C-OCIC, Avtech Electrosystems Ltd, Nepean, ON, Canada) were  
164 transmitted through a radiofrequency (RF) switch (Mini-Circuits, Brooklyn, NY, USA) to the  
165 transducer. Reflected ultrasound signals were collected by the same transducer, amplified by a 30  
166 dB amplifier (Model # AU-2A-0150, Narda-MITEQ, Hauppauge, NY, USA) then digitized at 625  
167 MS/s by 14-bit resolution A/D board (Teledyne SP Devices, Linköping, Sweden). At each  
168 location, signals were averaged 45 times to increase the signal-to-noise ratio and saved to a  
169 computer for offline processing and analysis using MATLAB (MathWorks, Natick, MA, USA).  
170 With a pulse repetition frequency of 10 kHz, the time to acquire data from a single raster scan was  
171 8 minutes. The acquisition system hardware was computer-controlled using a trigger card  
172 (SpinCore Technologies, Gainesville, FL, USA). The entire system was enclosed in a temperature-  
173 controlled incubator (In Vivo Scientific LLC, Salem, SC, USA).

174 US data acquisition was performed with a thin polymethyl-pentene film (DX-845 TPX, C.  
175 S. Hyde Company, Lake Villa, IL, USA) and with hydrogel samples for validation of the acoustic



176 characterization method (see below). Finally, cell-laden hydrogels were scanned and  
177 characterized. For TPX, the incubator temperature was set to 22°C, whereas for the hydrogel  
178 samples it was set to 37°C.

## 179 **2.3 Method validation**

180 To validate our method, the acoustic properties of a thin DX-845 grade TPX film were  
181 estimated and compared to those reported in [19] and [20]. The film was taped to a polystyrene  
182 Petri dish and covered with water at 22°C to match the temperature conditions of [19]. RF signals  
183 were collected as described in 2.2, and all material properties were calculated using equations (1)  
184 to (10), with  $c_w = 1488$  m/s [20],  $\rho_w = 997.77$  kg/m<sup>3</sup> [21],  $c_p = 2410$  m/s [22],  $\rho_p = 1050$  kg/m<sup>3</sup>  
185 (general purpose polystyrene) and resulting acoustic impedances  $Z_w = 1.485$  MRayl and  $Z_p =$   
186  $2.531$  MRayl. For the attenuation in water in equation (1), which can be expressed as  $\alpha_w(f) =$   
187  $af^2$ ,  $a$  was set to  $2.22 \times 10^{-4}$  dB/mm/MHz<sup>2</sup>. For comparison, the film thickness was measured  
188 using a spherical digital tube micrometer (Mitutoyo Canada Inc., Mississauga, CA) before the  
189 acoustic measurement.

190 Since sample thickness plays a critical role in evaluating the acoustic properties, the  
191 acoustic measurement of the thickness of fibrin hydrogel samples was compared to laser confocal  
192 microscopy measurement. To fabricate the fibrin hydrogel, equal volumes of fibrinogen (Sigma-  
193 Aldrich, CAT# F8630) solution in Dulbecco's phosphate-buffered saline (Gibco™ DPBS -/-,  
194 ThermoFisher Scientific, CAT# 14190144) and thrombin (Sigma-Aldrich, CAT# T6634) solution  
195 in complete cell culture medium were mixed to reach final concentrations of 5 mg/ml and 3 unit/ml  
196 for fibrinogen and thrombin, respectively. The mixture was cast in polydimethylsiloxane (PDMS)  
197 disk-shaped molds with a diameter of 8 mm (Fig. 1B) and initial thicknesses of 0.75 mm, 1.00  
198 mm, and 1.25 mm. The mixture was incubated at 37 °C and 100% humidity for 90 min for

199 crosslinking, after which DPBS  $+/+$  (Corning, CAT# 21-030-CV) was added, and US  
200 measurements were conducted. Then, fibrin gels were stained by exposure to 50  $\mu$ l of  
201 tetramethylrhodamine isothiocyanate (TRITC)–Dextran (Sigma-Aldrich – CAT# T1037) solution  
202 in DPBS  $+/+$  at a concentration of 5 mg/ml and incubation at 37 °C for 1 hr. The hydrogels were  
203 washed using DPBS  $+/+$ . Their thickness was measured using a laser confocal microscope  
204 (Olympus FV3000) with emission at 640 nm by focusing on the lowest and highest surfaces where  
205 a meaningful signal was detected at a single location. The distance between these two surfaces was  
206 taken as the hydrogel sample thickness and compared with US measurements (eq. 7), for which  
207 the speed of sound in DPBS at 37°C was assumed to be that of pure water at the same temperature  
208 ( $c_w = 1524$  m/s [21]). All the MATLAB processing codes, A-line data, statistical analyses, and  
209 selected ROIs are publicly available [here](#) for other researchers to reproduce the results of this study.

## 210 **2.4 Cell-laden hydrogel acoustic characterization**

211 Cell contraction can change the thickness and size of a cell-laden gel [13]. Although high-  
212 frequency US studies have examined cell-laden gels, cell contraction in hydrogels and engineered  
213 tissues have not been taken into account [7-11, 16, 17], despite the unavoidable effects on the  
214 physical and acoustic properties of these media. To address this issue, we seeded fibrin hydrogels,  
215 with initial thicknesses of 0.75, 1, and 1.25 mm, with cells at densities of  $1 \times 10^5$ ,  $1 \times 10^6$  and  $1 \times 10^7$   
216 cells/ml.

217 Cell-laden hydrogels were prepared using human umbilical perivascular cells (hUCPVC)  
218 (Tissue Regeneration Therapeutics Toronto, Ontario, Canada). Cells at passage three were cultured  
219 in T175 flasks (CAT# 431080, Corning Life Sciences®, Tewksbury, Massachusetts, United  
220 States) in Minimum Essential Medium (MEM) Alpha (Gibco™ MEM  $\alpha$ , CAT# 12561056,  
221 ThermoFisher Scientific, Mississauga, Ontario, Canada), at 37°C in an atmosphere of 5% CO<sub>2</sub>

222 and 100% humidity. MEM was supplemented with 20% v/v fetal bovine serum (Gibco™ FBS,  
223 CAT# 12483-020, ThermoFisher Scientific, Mississauga, Ontario, Canada), 0.24% v/v L-  
224 glutamine 200 mM (CAT# G7513, Sigma Aldrich, Oakville, Ontario, Canada), and 0.24% v/v  
225 penicillin-streptomycin 10,000 unit/ml (Gibco™, CAT# 15140122, ThermoFisher Scientific,  
226 Mississauga, Ontario, Canada). The culture medium was refreshed every three days. Then,  
227 hUCPVCs at passage four were suspended in the thrombin solution used in the hydrogel  
228 preparation described in section 2.3, before mixing with the fibrin solution. The final cell densities  
229 produced in hydrogel were  $1 \times 10^5$ ,  $1 \times 10^6$ , or  $1 \times 10^7$  cell/ml. Cell-laden hydrogels were then cultured  
230 in MEM for one day before US measurements.

231         Ultrasound data were acquired as described in section 2.2, and processed as in section 2.1,  
232 with the assumptions that the attenuation, speed of sound and density of MEM and DPBS were  
233 equal to those of water at 37°C (i.e.,  $c_w = 1524$  m/s [21],  $\rho_w = 993.33$  kg/m<sup>3</sup> [22], and  $a =$   
234  $1.39 \times 10^{-4}$  dB/mm/MHz<sup>2</sup>). As for the polystyrene substrate, its speed of sound was set to  $c_p =$   
235  $2380$  m/s [23], and its density is assumed to be unchanged relative to 22°C ( $\rho_p = 1050$  kg/m<sup>3</sup>) due  
236 to the material's low expansion coefficient. The resulting acoustic impedances for coupling  
237 medium and polystyrene were therefore set to  $Z_w = 1.513$  MRayl and  $Z_p = 2.499$  MRayl. The  
238 average standard deviations for the thickness and speed of sound across the entire gel ROI area is  
239 provided in Supplementary Table 1. The average standard deviation in thickness and speed of  
240 sound across the selected 6 mm ROI for an entire gel across all cell conditions was 38  $\mu$ m and 5  
241 m/s which is <7% of the mean thickness values <1% of the mean speed of sound values  
242 (Supplementary Table 1).

## 243 **2.7 Statistical analyses**

244 Results are presented as mean  $\pm$  standard deviation of the acoustic, physical, or mechanical  
245 properties measured over the ROI for each fibrin gel. Measurements were performed in three to  
246 six different samples for each cell density and each sample thickness. A one-way ANOVA was  
247 used to evaluate the significance of the differences in the means of all measured properties between  
248 cell concentrations, with pairwise comparisons using Tukey's multiple comparisons test ( $\alpha =$   
249 0.001) (GraphPad Prism v8.0, San Diego, USA). Correlations of the speed of sound and acoustic  
250 attenuation coefficient with thickness were tested by performing a two-tailed Pearson's correlation  
251 analysis with  $\alpha = 0.01$ .

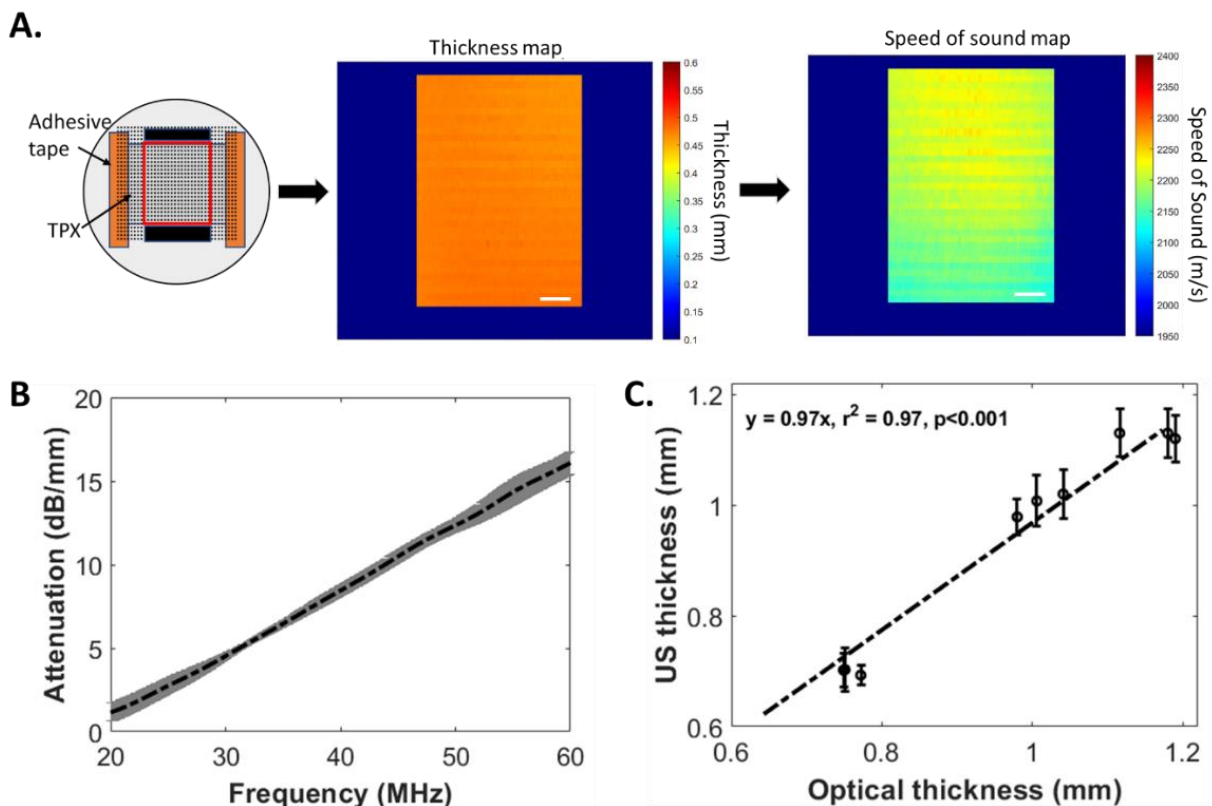
## 252 **3 Results**

### 253 **3.1 Acoustic characterization validation**

254 Speed of sound, acoustic impedance, density, and acoustic attenuation coefficient of TPX  
255 estimated using the method described in sections 2.1 and 2.2, are compared to those obtained using  
256 other measurement methods in Table 1. We found strong agreement between measured and  
257 reference values, with a maximum difference of 6.6% (Fig. 2, Table 1). To further validate our  
258 technique, we measured the thickness of cell-free fibrin gels in comparison with laser confocal  
259 microscopy and found that the thicknesses of cell-free fibrin gels measured by US were highly  
260 correlated with those measured by confocal microscopy ( $r^2=0.97$ ;  $p<0.001$ ; Fig. 2C).

Property	Measured value	Reference value	Percent difference	Ref.
Thickness (mm)	$0.472 \pm 0.004$	$0.465 \pm 0.001$	1.5%	Measured via digital tube micrometer
Speed of sound (m/s)	$2180 \pm 14$ @ 22°C	2093	4.1%	[19]
		2190	0.5%	[20]
Acoustic impedance (MRayl)	$1.70 \pm 0.01$	$^{\S}1.7, 1.83$	-	[20]
Density (kg/m <sup>3</sup> )	$778 \pm 8$	833	6.6 %	[19]
Acoustic attenuation @ 40 MHz (dB/mm)	$8.44 \pm 0.24$ (DX-845 film)	776	0.3%	[20]
		$^*11.94$ (RT-18 film)	-	[19]
		$^*9.74$ (DX-845 sheet)		

261  
 262 **Table 1:** Properties of the TPX film at 22°C ( $\pm$  standard deviation, n=3) compared to published  
 263 reference values from two studies [19] and [20]. Percent differences for some values are calculated  
 264 based on the furthest reference value to the measured value from either [19] and/or [20].<sup>§</sup>Acoustic  
 265 impedance values are presented using two different methods in [20] and thus cannot be directly  
 266 compared and are not published in [19]. <sup>\*</sup>Acoustic attenuation was calculated via a mean  
 267 maximum amplitude time domain method and cannot be directly compared with our analytical  
 268 method. Further discussion of both these discrepancies is presented in the Discussion section.

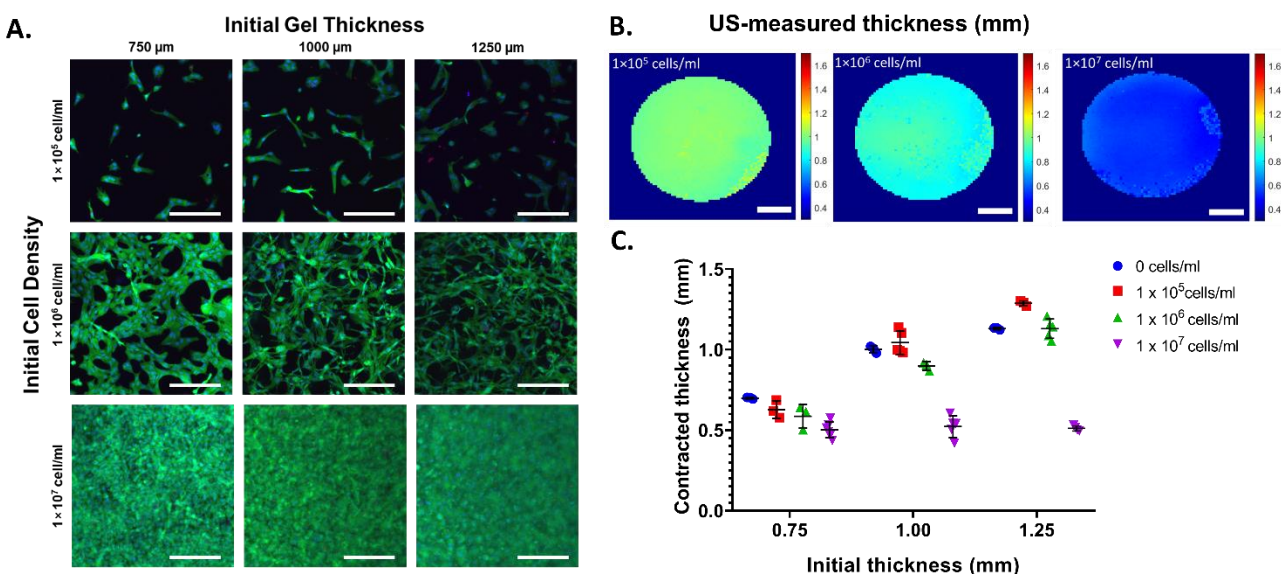


269  
 270 **Figure 2:** (A-left) TPX film taped down to a polystyrene Petri dish. Dotted lines represent the data  
 271 acquisition raster scan, with the red line delimiting the ROI used for sample acoustic  
 272 characterization, and the black rectangles representing the ROIs where the substrate reference  
 273 signals were collected. (A-middle) estimated local sample thickness. (A-right) local speed of  
 274 sound. Scale bars = 2 mm. (B) TPX frequency-dependent attenuation. (C) Cell-free fibrin gel  
 275 thickness: US vs confocal microscopy (error bars: spatial standard deviation of US measurements  
 276 over the ROI, dashed line: linear fit).

## 277 3.2 Effects of cell-mediated contraction on physical properties of cell-

## 278 laden hydrogels

279 Optical images of cell-laden hydrogels of different thickness and at different cell concentrations  
280 are shown on Fig. 3A, showing visual changes in the population of cells in the fibrin hydrogels at  
281 each cell condition. Ultrasound measurements showed a spatially uniform shrinkage of the  
282 hydrogel associated with cell contraction (Fig. 3B). The standard deviation of the thickness  
283 measurements is shown in Supplementary Table 1. This shrinkage increases with cell density, with  
284 as much as 60% reduction in the thickness for hydrogels seeded with  $1 \times 10^7$  cell/ml relative to their  
285 initial thickness (Fig. 3C).



286  
287 **Figure 3** – (A) Optical images of cell-laden hydrogels of three different initial thicknesses  
288 (columns) and at three different cell densities (rows). Live cells, green; dead cells, red; nucleus,  
289 blue. Scale bars = 200  $\mu\text{m}$ . (B) US-measured thicknesses of hydrogels of 1.00 mm initial thickness,  
290 with cell densities of, from left to right,  $1 \times 10^5$ ,  $1 \times 10^6$  and  $1 \times 10^7$  cell/ml. Scale bars = 1 mm. (C)  
291 Effect of cell contraction on hydrogel thickness measured via US compared to the initial hydrogel  
292 thickness.

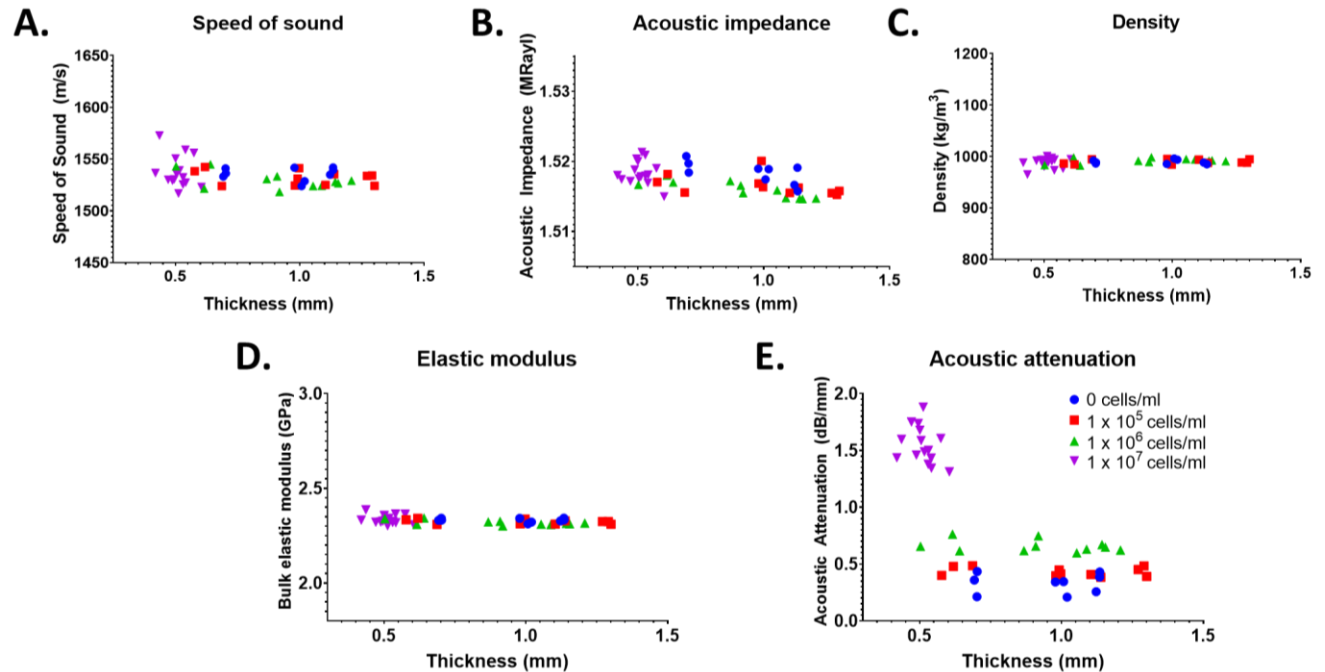
293  
294 Variations in hydrogel thickness, such as those induced by cell contraction, can confound acoustic  
295 property measurements if the thickness is not measured accurately in situ. Furthermore, reported

296 acoustic attenuation estimation methods [7-12, 16, 17], which did not compensate for local losses  
297 associated with reflection and transmissions at interfaces, introduce a thickness-dependent bias  $b$ ,  
298 in the estimated attenuation coefficient, which is expressed as:

$$299 \quad b(d) = \frac{1}{2d} \cdot 20 \log_{10} \left[ \frac{R_{w-p}}{R_{s-p} \cdot T_{w-s}^2} \right] \quad (11)$$

300 This bias can become significant for small sample thicknesses and is presented for all measured  
301 samples in Supplementary Table 2.

302 To evaluate whether the method could overcome the aforementioned limitations, we investigated  
303 the thickness dependence of the acoustic properties of cell-laden hydrogels. Results summarized  
304 in Fig. 4 demonstrate that speed of sound, acoustic attenuation, density, and elastic modulus were  
305 not significantly correlated with gel thickness over a wide range of cell densities and gel  
306 thicknesses (Fig. 4;  $p > 0.11$ ,  $p > 0.23$ ,  $p > 0.22$ ,  $p > 0.05$  across cell densities via Pearson's,  
307 respectively). Acoustic impedance was only statistically correlated with thickness in the  $1 \times 10^6$   
308 cell/ml condition ( $p < 0.01$ ,  $r = -0.85$ ), but with weak dependency as values varied by  $< 0.2\%$  across  
309 seven orders of magnitude of cell density (corresponding to minor absolute differences of  $\sim 0.002$   
310 MRayl).



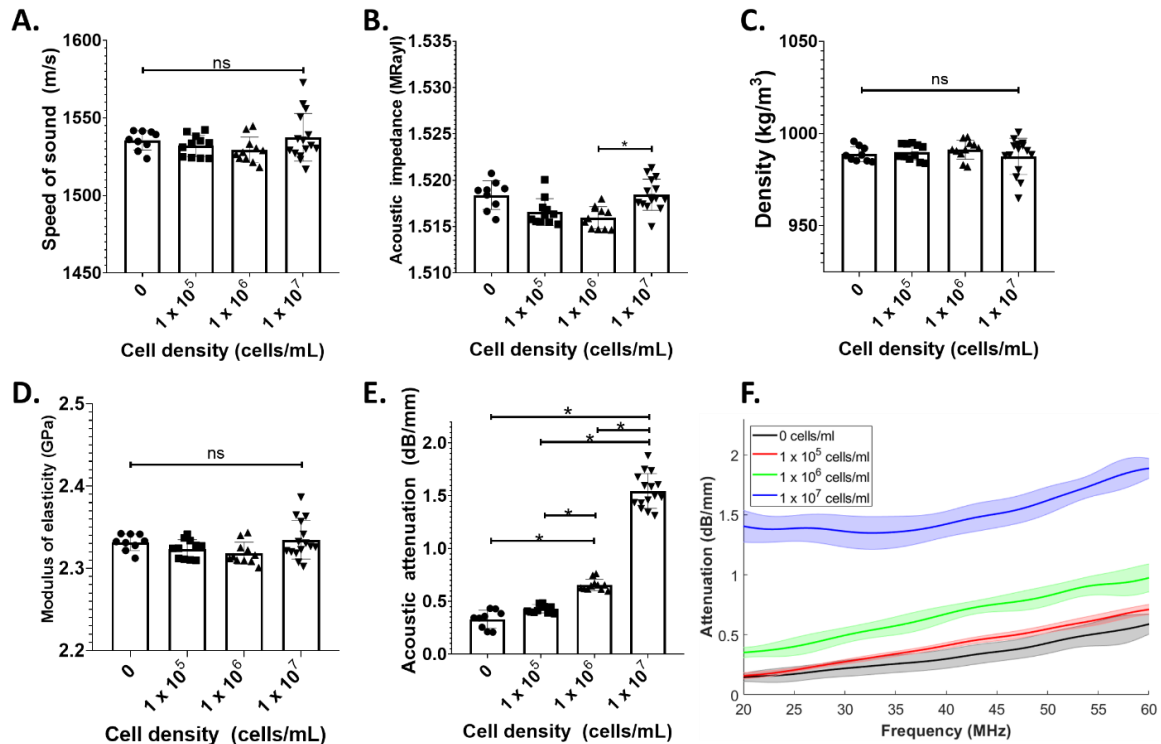
311  
312 **Figure 4:** Thickness dependence of (A) speed of sound, (B) acoustic impedance, (C) acoustic  
313 attenuation, (D) density, and (E) elastic modulus. None of the properties were significantly  
314 correlated with hydrogel thickness ( $p > 0.01$ ; Pearson's), except for a weak correlation for  
315 acoustic impedance at  $1 \times 10^6$  cell/ml ( $p < 0.01$ ;  $r = -0.85$ ).  
316

### 317 **3.3 Acoustic properties of cell-laden hydrogels**

318 Since thickness was determined to be a non-confounding factor in our method (Fig. 4), cell density  
319 in these cell-laden hydrogels can be considered the primary factor driving affecting the acoustic  
320 attenuation coefficient. The acoustic properties (e.g., speed of sound, acoustic impedance, acoustic  
321 attenuation coefficient), density, and elastic modulus of cell-laden gels ( $n=46$ ) are reported as a  
322 function of initial cell density in Figure 5 (summarized in Supplementary Table 1). There were no  
323 statistically significant difference in the speed of sound across cell densities, with  $<0.6\%$  difference  
324 between the mean values ( $p=0.25$ ; Fig. 5A). Similarly, acoustic impedance measurements varied  
325 by  $<0.2\%$  across cell densities, although a statistical difference was detected between the two  
326 highest cell densities (Fig. 5B). Since speed of sound and impedance are mostly invariant with cell  
327 density in the fibrin gels, the derived density and elastic modulus varied minimally across cell



328 densities. The mean densities of the fibrin hydrogels (988 – 991 kg/m) were approximately those  
 329 of water [21], with no significant differences across cell densities (Fig. 5C;  $p>0.59$ ). Similarly,  
 330 elastic modulus measurements varied by less than  $<0.7\%$  across cell densities (corresponding to  
 331 absolute differences of  $<0.02$  GPa), with no significant differences across cell densities (Fig. 5D;  
 332  $p>0.08$ ). In contrast, the acoustic attenuation coefficient measured at 40 MHz increased  
 333 significantly with increasing cell density (Fig. 5E;  $p<0.001$ ), except between cell-free and  $1\times 10^5$   
 334 cell/ml. This increase is observed across the bandwidth of the transducer (20 – 60 MHz) as shown  
 335 in Figure 5F.



336  
 337 **Figure 5:** Measurements of the acoustic properties of cell-laden hydrogels at four different cell  
 338 densities and three thicknesses, including (A) speed of sound and (B) acoustic impedance via our  
 339 ultrasound method, (C) density and (D) modulus of elasticity derived from the values in (A-B),  
 340 and (E) acoustic attenuation at 40 MHz. (F) Representative frequency-dependent attenuation plot  
 341 for each cell density in a 1.00 mm gel within the bandwidth of the transducer (20-60 MHz).  
 342 Standard deviations at each frequency are represented as shaded areas around the mean  
 343 attenuation. A minimum of  $n=3$  independent gels were used per thickness for each initial cell  
 344 density. Non-significant (ns) statistical differences between groups by a one-way ANOVA are  
 345 shown and significant differences from a post-hoc Tukey's multiple comparison test are shown  
 346 with  $*p < 0.001$ .

## 347 **4 Discussion**

348 US has excellent potential for non-invasive, real-time monitoring of the acoustic, physical, and  
349 mechanical properties of biomaterials and engineered tissues. Here, we developed an analytical  
350 approach that addresses the limitations of previous approaches and validated it by measuring the  
351 acoustic properties of TPX. We then applied this technique in cell-laden fibrin hydrogels.  
352 Importantly, our approach accurately measured hydrogel thickness, despite significant cell-  
353 mediated contraction, which enabled estimations of acoustic properties that were effectively  
354 independent of thickness and reflected intrinsic hydrogel properties.

355 Since sample thickness plays a critical role in evaluating the acoustic properties, the acoustic  
356 measurement of the thickness of TPX and fibrin hydrogel samples was compared to a digital tube  
357 micrometer and a laser confocal microscopy measurement, respectively, and good agreement was  
358 found. To validate our acoustic measurement technique, we compared the physical and acoustic  
359 properties of TPX at 40 MHz obtained using our analytical approach to those obtained with the  
360 methods used by Madsen et al [19] and Bloomfield et al [20]. The speed of sound determined via  
361 our method was within range of the speed determined in [19] and [20]. Bloomfield et al. [20]  
362 present two acoustic impedance values for TPX for two different measurement methods. Using  
363 reflection coefficient measurements, Bloomfield et al. also calculate an acoustic impedance of  
364 TPX of 1.7 MRayl which is consistent with our measurements (Table 1). However, using a  
365 measured speed of sound and a manufacturer-provided density, Bloomfield et al. determine the  
366 acoustic impedance of TPX to be 1.83 MRayl. The latter method is less accurate as it relies on a  
367 non-experimentally derived value but was incorrectly used for density calculations. Instead of  
368 using the manufacturer-provided density, if Bloomfield et al. had used the pulse-echo-measured  
369 impedance (1.7 MRayl) and their measured speed of sound (2190 m/s) to estimate the density of

370 TPX, their obtained value would have been  $776 \text{ kg/m}^3$  which is within  $<1\%$  of our study's  
371 measured density (Table 1). With regards to attenuation, we found a difference between our  
372 measurements and those from [19], and [20], which is most likely due to the difference in  
373 measurement approaches used in each study. One should note that in materials for which  
374 attenuation is highly dependent on frequency, such as TPX, broad-band time domain amplitude  
375 measurement methods ([19, 20]) are suboptimal due to downshift of the central frequency of the  
376 ultrasound pressure pulse signal propagating through the sample. Moreover, from Eq.11, there is  
377 a bias of 2.58 dB/mm when local losses associated with reflection and transmissions at the  
378 interfaces are not accounted for. Through addition of this bias to our measurement of the acoustic  
379 attenuation of TPX at 40 MHz of 8.44 dB/mm, we are within range of [19]. Nevertheless, the  
380 acoustic attenuation measured by our largely frequency-based approach should be more accurate  
381 than [19] across different sample types because it accounts for changes in the peak frequency of  
382 the media rather than the ratio of the amplitude of the time-domain signals.

383 Of the acoustic properties measured, the acoustic attenuation coefficient had the most notable  
384 change with increased cell density. Our acoustic attenuation coefficient values are within range of  
385 other published studies [8, 9, 16, 17], which have not accounted for all physical interfacial  
386 phenomena. The average bias for cell-laden hydrogels is 0.03 dB/mm (Supplementary Table 2)  
387 because the acoustic impedance of the fibrin hydrogels is similar to that of the coupling liquid.  
388 However, for: 1) thicker engineered tissues or implantable biomaterials, this bias would be  
389 prominent; and 2) for stiffer engineered tissues (e.g., cartilage, bone), this acoustic impedance  
390 mismatch would be higher and cause the bias to have more significant effects. As the fibrin  
391 hydrogels were  $>99\%$  water, the measured speed of sound, derived density, and derived bulk  
392 modulus of the gels were approximately that of water at  $37^\circ\text{C}$  ( $1524 \text{ m/s}$ ,  $993.33 \text{ kg/m}^3$ ,  $2.32 \text{ GPa}$

393 from Eq. 8, respectively). We did not expect the addition of cells within the fibrin hydrogels to  
394 affect the speed of sound, acoustic impedance, density, and elastic modulus (assuming no shear  
395 propagation) of the cell-laden fibrin hydrogels since cells are largely ( $\geq 70\%$  [25]) composed of  
396 water with a high concentration of salt and have properties that approach those of 37°C water [26].  
397 In contrast, acoustic impedance increased with cell density ostensibly due to absorption and  
398 scattering by the cells' lipidic membranes [27] and nuclei [14], respectively.

399 Our study has limitations: (1) Our method calculates acoustic impedance using the reflection  
400 coefficient at the water-sample interface as a ratio between the pulse-echo signal from the water-  
401 substrate interface and the water-sample interface. As such, it is sensitive to local variations in the  
402 interface topography, e.g., due to focal cell topography, contraction, or swelling. (2) Non-uniform  
403 distribution of cells through the thickness of the fibrin hydrogels could lead to underestimation of  
404 the attenuation values, as Eq.1 is normalized to the thickness of the entire gel ( $d$ ) rather than to the  
405 thickness of where the dominant population of cells are located during the actual measurement.  
406 (3) Lastly, although our technique is versatile and can be used with any substrate material of known  
407 acoustic properties, it requires good adherence of the sample to the substrate to avoid air gaps  
408 between the sample and substrate. However, regardless of the substrate and/or sample material,  
409 the frequency-based approach presented in this study can be used to estimate the acoustic  
410 properties of cell-laden hydrogels across multiple thicknesses and cell densities. In future work,  
411 the approach could be used to monitor dynamics changes with culture time.

## 412 **5 Conclusion**

413 Here, we present a non-invasive and non-destructive high-frequency quantitative US  
414 method to estimate the acoustic, physical, and mechanical properties of biomaterials and

415 engineered tissues with high resolution (~100  $\mu\text{m}$ ). This method accounts for all physical  
416 interfacial phenomena to estimate the intrinsic physical and acoustic properties of cell-laden  
417 hydrogels, including thickness, speed of sound, acoustic impedance, acoustic attenuation  
418 coefficient, density, and elastic modulus, without the confounding variable of hydrogel thickness.  
419 We showed that increased cell density in the hydrogel led to an increase in the acoustic attenuation  
420 coefficient, demonstrating the ability of high-frequency US to detect changes in the cellularity of  
421 cell-laden biomaterials. Importantly, the method corrects for changes in hydrogel thickness due to  
422 cell-mediated contraction. This robust technique enables non-invasive, non-destructive estimation  
423 of the acoustic, physical, and mechanical properties of cell-laden biomaterials at spatial resolutions  
424 that are relevant for tissue engineering applications.

## 425 **6 Acknowledgements**

426 This work was supported by a Collaborative Health Research Program grant from the Natural  
427 Science and Engineering Research Council of Canada (NSERC; CHRPI 5083) and Canadian  
428 Institutes of Health Research (CPG-151946). J.A.S was supported by an NSERC Canada Graduate  
429 Scholarship – Master’s, a CRAFT Doctoral Fellowship, an NSERC CREATE Doctoral  
430 Fellowship, and an NSERC Vanier Canada Graduate Scholarship. E.M.S was supported by an  
431 NSERC postdoctoral scholarship and a Medicine by Design Postdoctoral Fellowship. B.M. was  
432 supported by an NSERC Canada Graduate Scholarship – Doctoral.

## 433 **7 Data availability**

434 The raw data and codes to process the raw data required to reproduce these findings of this study  
435 are available to download from [here](#).

## 436 **8 References**

- 437 [1] Dalecki, D., & Hocking, D. C. (2016). Advancing Ultrasound Technologies for Tissue  
438 Engineering. In *Handbook of Ultrasonics and Sonochemistry* (pp. 1101–1126). Springer  
439 Singapore. [https://doi.org/10.1007/978-981-287-278-4\\_28](https://doi.org/10.1007/978-981-287-278-4_28)
- 440 [2] Kim, K., & Wagner, W. R. (2016). Non-invasive and Non-destructive Characterization of  
441 Tissue Engineered Constructs Using Ultrasound Imaging Technologies: A Review. *Annals of*  
442 *Biomedical Engineering*, 44(3), 621–635. <https://doi.org/10.1007/s10439-015-1495-0>
- 443 [3] Dalecki, D., Mercado, K. P., & Hocking, D. C. (2016). Quantitative Ultrasound for  
444 Nondestructive Characterization of Engineered Tissues and Biomaterials. *Annals of*  
445 *Biomedical Engineering*, 44(3), 636–648. <https://doi.org/10.1007/s10439-015-1515-0>
- 446 [4] Deng, C. X., Hong, X., & Stegemann, J. P. (2016). Ultrasound Imaging Techniques for  
447 Spatiotemporal Characterization of Composition, Microstructure, and Mechanical Properties  
448 in Tissue Engineering. *Tissue Engineering Part B: Reviews*, 22(4), 311–321.  
449 <https://doi.org/10.1089/ten.teb.2015.0453>
- 450 [5] Dalecki, D., & Hocking, D. C. (2015). Ultrasound Technologies for Biomaterials Fabrication  
451 and Imaging. *Annals of Biomedical Engineering*, 43(3), 747–761.  
452 <https://doi.org/10.1007/s10439-014-1158-6>
- 453 [6] Aliabouzar, M., Zhang, G. L., & Sarkar, K. (2018). Acoustic and mechanical characterization  
454 of 3D-printed scaffolds for tissue engineering applications. *Biomedical Materials*, 13(5),  
455 055013. <https://doi.org/10.1088/1748-605X/aad417>
- 456 [7] Cafarelli, A., Verbeni, A., Poliziani, A., Dario, P., Menciassi, A., & Ricotti, L. (2017). Tuning  
457 acoustic and mechanical properties of materials for ultrasound phantoms and smart substrates

- 458 for cell cultures. *Acta Biomaterialia*, 49, 368–378.  
459 <https://doi.org/10.1016/j.actbio.2016.11.049>
- 460 [8] Mercado, K. P., Helguera, M., Hocking, D. C., & Dalecki, D. (2015). Noninvasive  
461 Quantitative Imaging of Collagen Microstructure in Three-Dimensional Hydrogels Using  
462 High-Frequency Ultrasound. *Tissue Engineering Part C: Methods*, 21(7), 671–682.  
463 <https://doi.org/10.1089/ten.tec.2014.0527>
- 464 [9] Ruland, A., Gilmore, K. J., Daikuara, L. Y., Fay, C. D., Yue, Z., & Wallace, G. G. (2019).  
465 Quantitative ultrasound imaging of cell-laden hydrogels and printed constructs. *Acta*  
466 *Biomaterialia*, 91, 173–185. <https://doi.org/10.1016/j.actbio.2019.04.055>
- 467 [10] Gudur, M. S. R., Rao, R. R., Peterson, A. W., Caldwell, D. J., Stegemann, J. P., & Deng, C.  
468 X. (2014). Noninvasive Quantification of In Vitro Osteoblastic Differentiation in 3D  
469 Engineered Tissue Constructs Using Spectral Ultrasound Imaging. *PLoS ONE*, 9(1), e85749.  
470 <https://doi.org/10.1371/journal.pone.0085749>
- 471 [11] Mercado, K. P., Helguera, M., Hocking, D. C., & Dalecki, D. (2014). Estimating Cell  
472 Concentration in Three-Dimensional Engineered Tissues Using High Frequency Quantitative  
473 Ultrasound. *Annals of Biomedical Engineering*, 42(6), 1292–1304.  
474 <https://doi.org/10.1007/s10439-014-0994-8>
- 475 [12] D’Astous, F. T., & Foster, F. S. (1986). Frequency dependence of ultrasound attenuation and  
476 backscatter in breast tissue. *Ultrasound in Medicine & Biology*, 12(10), 795–808.  
477 [https://doi.org/10.1016/0301-5629\(86\)90077-3](https://doi.org/10.1016/0301-5629(86)90077-3)
- 478 [13] Strohm, E. M., Czarnota, G. J., & Kolios, M. C. (2010). Quantitative measurements of  
479 apoptotic cell properties using acoustic microscopy. *IEEE Transactions on Ultrasonics*,

- 480 Ferroelectrics and Frequency Control, 57(10), 2293–2304.  
481 <https://doi.org/10.1109/TUFFC.2010.1690>
- 482 [14] Taggart, L. R., Baddour, R. E., Giles, A., Czarnota, G. J., & Kolios, M. C. (2007). Ultrasonic  
483 Characterization of Whole Cells and Isolated Nuclei. *Ultrasound in Medicine & Biology*,  
484 33(3), 389–401. <https://doi.org/10.1016/j.ultrasmedbio.2006.07.037>
- 485 [15] Vernerey, F. J., Lalitha Sridhar, S., Muralidharan, A., & Bryant, S. J. (2021). Mechanics of  
486 3D Cell–Hydrogel Interactions: Experiments, Models, and Mechanisms. *Chemical Reviews*,  
487 121(18), 11085–11148. <https://doi.org/10.1021/acs.chemrev.1c00046>
- 488 [16] Ruland, A., Hill, J. M., & Wallace, G. G. (2021). Reference Phantom Method for Ultrasonic  
489 Imaging of Thin Dynamic Constructs. *Ultrasound in Medicine & Biology*, 47(8), 2388–2403.  
490 <https://doi.org/10.1016/j.ultrasmedbio.2021.04.014>
- 491 [17] Ruland, A., Onofrillo, C., Duchi, S., Di Bella, C., & Wallace, G. G. (2022). Standardised  
492 quantitative ultrasound imaging approach for the contact-less three-dimensional analysis of  
493 neocartilage formation in hydrogel-based bioscaffolds. *Acta Biomaterialia*, 147, 129–146.  
494 <https://doi.org/10.1016/j.actbio.2022.05.037>
- 495 [18] Briggs, G. A. D., Wang, J., & Gundle, R. (1993). Quantitative acoustic microscopy of  
496 individual living human cells. *Journal of Microscopy*, 172(1), 3–12.  
497 <https://doi.org/10.1111/j.1365-2818.1993.tb03387.x>
- 498 [19] Madsen, E. L., Deaner, M. E., & Mehi, J. (2011). Properties of Phantom Tissue-like  
499 Polymethylpentene in the Frequency Range 20–70 MHz. *Ultrasound in Medicine & Biology*,  
500 37(8), 1327–1339. <https://doi.org/10.1016/j.ultrasmedbio.2011.05.023>
- 501 [20] Bloomfield, P. E., Wei-Jung Lo, & Lewin, P. A. (2000). Experimental study of the  
502 acoustical properties of polymers utilized to construct PVDF ultrasonic transducers and the



- 503 acousto-electric properties of PVDF and P(VDF/TrFE) films. *IEEE Transactions on*  
504 *Ultrasonics, Ferroelectrics and Frequency Control*, 47(6), 1397–1405.  
505 <https://doi.org/10.1109/58.883528>
- 506 [21] Del Grosso, V. A., & Mader, C. W. (1972). Speed of Sound in Pure Water. *The Journal of*  
507 *the Acoustical Society of America*, 52(5B), 1442–1446. <https://doi.org/10.1121/1.1913258>
- 508 [22] Haynes, W. M. (2014). *CRC handbook of chemistry and physics: A ready-reference book of*  
509 *chemical and physical data*.
- 510 [23] Kono, R. (1960). The Dynamic Bulk Viscosity of Polystyrene and Polymethyl Methacrylate.  
511 *Journal of the Physical Society of Japan*, 15(4), 718–725.  
512 <https://doi.org/10.1143/JPSJ.15.718>
- 513 [24] Treeby, B. E., Zhang, E. Z., Thomas, A. S., & Cox, B. T. (2011). Measurement of the  
514 Ultrasound Attenuation and Dispersion in Whole Human Blood and its Components From 0–  
515 70 MHz. *Ultrasound in Medicine & Biology*, 37(2), 289–300.  
516 <https://doi.org/10.1016/j.ultrasmedbio.2010.10.020>
- 517 [25] Cooper GM. *The Cell: A Molecular Approach*. 2nd edition. Sunderland (MA): Sinauer  
518 Associates; 2000. The Molecular Composition of Cells.
- 519 [26] Wirtzfeld, L. A., Berndl, E. S. L., Czarnota, G. J., & Kolios, M. C. (2017). Monitoring  
520 Quantitative Ultrasound Parameter Changes in a Cell Pellet Model of Cell Starvation.  
521 *Biophysical Journal*, 112(12), 2634–2640. <https://doi.org/10.1016/j.bpj.2017.05.017>
- 522 [27] Sundaram, J., Mellein, B. R., & Mitragotri, S. (2003). An Experimental and Theoretical  
523 Analysis of Ultrasound-Induced Permeabilization of Cell Membranes. *Biophysical Journal*,  
524 84(5), 3087–3101. [https://doi.org/10.1016/S0006-3495\(03\)70034-4](https://doi.org/10.1016/S0006-3495(03)70034-4)